

# Dynamic compression of highly compressible porous media with application to snow compaction

By Q. WU†, Y. ANDREOPOULOS, S. XANTHOS  
AND S. WEINBAUM‡

Departments of Biomedical and Mechanical Engineering and New York Center for Biomedical Engineering, The City College of the City University of New York, New York, NY 10031, USA

(Received 2 June 2004 and in revised form 31 May 2005)

A new experimental and theoretical approach is presented to examine the dynamic lift forces that are generated in the compression of both fresh powder snow and wind-packed snow. At typical skiing velocities of 10 to 30 ms<sup>-1</sup> the duration of contact of a ski or snowboard with the snow will vary from 0.05 to 0.2 s depending on the length of the planing surface and its speed. No one, to our knowledge, has previously measured the dynamic behaviour of snow on such a short time scale and, thus, there are no existing measurements of the excess pore pressure that can build-up in snow on this time scale. Using a novel porous cylinder–piston apparatus, we have measured the excess pore pressure that would build-up beneath the piston surface and have also measured its subsequent decay due to the venting of the air from the snow at the porous wall of the cylinder. In further experiments, in which the air is slowly and deliberately drained to avoid a build-up in pore pressure, we have been able to separate out the force exerted by the ice crystal phase as a function of its instantaneous deformation. A theoretical model for the pore pressure relaxation in the porous cylinder is then developed using consolidation theory. Dramatically different dynamic behaviour is observed for two different snow types, one (wind-packed) giving a steady continuous relaxation of the excess pore pressure and the other (fresh powder) leading to a piston rebound with negative pore pressure. A feature of the rebound is the apparent debonding of sintered ice crystals after maximum compression. This behaviour is described well by introducing a debonding coefficient where the debonding force is proportional to the expansion velocity of the medium. The experimental and theoretical approach presented herein and the previous generalized lubrication theory for compressible porous media, have laid the foundation for understanding the detailed dynamic response of soft porous layers to rapid deformation.

---

## 1. Introduction

In this paper, we shall examine the dynamic compaction of a snow layer whose thickness is typical of the snow blanket that is left after a single snowfall in many regions of the USA. We wish to understand the dynamic pore pressures that might build-up in a new snow layer on the time scale of loading associated with

† Current address: Department of Mechanical Engineering, Villanova University, 800 Lancaster Ave, Villanova, PA 19085, USA.

‡ Author to whom correspondence should be addressed: weinbaum@ccny.cuny.edu.

skiing, snowboarding or snow-shoeing. This is roughly 0.05 to 0.20 s in the first two applications and 0.5 s in the last application. A specially designed porous-walled cylinder–piston apparatus has been constructed to examine the build-up and decay of the excess pore pressure on these time scales, in two basic snow types, fresh and wind-blown snow. The idealized experimental apparatus is not intended to reproduce realistically the boundary conditions that we encounter in these applications. In skiing or snowboarding we must also consider the permeability of the base layer on which the latest snowfall rests, shear forces in the snow at the edge of the planform and the lateral displacement and momentum of the displaced snow, especially during turns and manoeuvring. However, this initial study does qualitatively and quantitatively explore the time variation of the various dynamic forces encountered when a weighted planar surface is suddenly dropped onto a snow layer before it is supported by the pressure bulb that develops in the ice crystal phase once quasi-steady longer time settling is achieved (Shoop & Alger 1998). The stress-density relationships for undisturbed low-density snow and disturbed higher-density snow, when subjected to various rates of loading ranging from 0 to  $40 \text{ cm s}^{-1}$ , have been studied at temperatures varying from  $-1^\circ\text{C}$  to  $-34^\circ\text{C}$  by Abele & Gow (1975, 1976). However, to our knowledge, the current study is the first experimental and theoretical investigation of pore-pressure generation inside a snow layer on the time scale of skiing or snowboarding.

An earlier theoretical investigation, Feng & Weinbaum (2000, hereinafter referred to as FW), showed that there was a remarkable hydrodynamic similarity between (a) the motion of a red blood cell (RBC) gliding at  $<20 \mu\text{m s}^{-1}$  on a compressed endothelial surface layer (ESL) of sulfated proteoglycans and glycoproteins that line the endothelial cells (EC) of human capillaries and (b) a skier or snowboarder sliding on soft snow powder, even though their difference in mass is of the order  $10^{15}$ . At velocities  $>20 \mu\text{m s}^{-1}$  the red blood cell rises out of the ESL and there is an intervening thin fluid lubricating layer between the ESL and the RBC membrane. FW predict that the excess pore pressure generated by a planing surface moving on any compressible porous media scales as  $\alpha^2 = h^2/K$ , where  $h$  is the layer thickness and  $K$  is the Darcy permeability. The theory in FW predicts that  $\alpha$  is of the order  $10^2$  or larger for both red blood cells gliding on the ESL and humans skiing. Thus, the lift forces generated can be four or more orders of magnitude greater than classical lubrication theory would predict. The huge enhancement in the lift arises because as the matrix compresses, there is a dramatic increase in the lubrication pressure owing to the marked increase in the hydraulic resistance that the fluid encounters as it tries to escape from the confining boundaries through the thin compressed porous layer.

The theoretical approach developed herein, as far as we are aware, has never been applied before to snow. It is based on consolidation theory first proposed by Terzaghi (1943) and refined in the more general theory of Biot (1941; Biot & Willis 1957) for two- and three-dimensional compression of a porous medium. Our experiments indicate that the time scale of the build-up in pore pressure of the air after dropping the piston varies between 0.05 s and 0.1 s, depending on the permeability of the snow, and that the decay time can be as much as five times longer than this if the maximum pore pressure is sufficient to bear the entire weight of the piston. However, the critical frequency for the propagation of pressure waves in a porous medium of infinite depth appears to be of the order of 100 kHz if we employ the present data in the acoustic theory of Albert (1993) and Johnson (1982). Thus, the imposition of the pressure field through the fast compressive wave and the multiple reflections of this wave occur on a much shorter time scale than the viscous phenomena we are investigating. Both the build-up and the drainage of the pore pressure within the cylinder exhibit a time-dependent

quasi-steady behaviour that is governed by Darcy's law, the instantaneous supporting force of the ice crystal structure and the conservation of mass for both the air and the solid phase. The weight of the piston is balanced by its inertia, the time-varying integrated pressure force of the transiently trapped air and the supporting force of the ice crystals. The latter is determined from a separate experiment in which small weights are gradually added to a lightweight piston and the compression of the snow measured as a function of the applied force until the full weight of the piston in the dynamic experiment is achieved. We found that the maximum compression depends on the microstructure of the snow, but if the compression is scaled relative to the maximum compression and the force relative to the maximum force, the dimensionless empirical relation was approximately the same for our fresh powder snow and the compression tests of Yong & Fukue (1977) on more dense snow. The theoretical model is, therefore, able to predict the time-dependent variation of each force if we can estimate the change in permeability of the snow as a function of its compression. Shimizu's (1970) empirical relation is used for this purpose.

Whereas there is an extensive literature on the behaviour of snow during uniaxial compression (see reviews by Mellor 1964, 1977; Shapiro *et al.* 1997), these studies largely address the compaction of snow and its creeping behaviour on much longer time scales, minutes and hours, rather than the short time scales of interest herein. On these time scales, a pressure bulb forms in the ice crystal structure and the weight is entirely supported by the solid phase. The mechanics of the initial nearly instantaneous compaction was of little interest to these authors since they were primarily concerned with the load-bearing capacity of snow as a more permanent supporting structure and the changing microstructure of the snow as a function of ageing and load application. In sharp contrast, in snowboarding on unpacked snow (not piste snow or prepared, already compressed surfaces), we are interested in the short-lived initial compression and the changing distribution of the load between the excess pore pressure and the compression of the solid phase before creep begins.

Another behaviour that was observed during the rebound of the piston for fresh powder snow (ambient temperature,  $T = -4^{\circ}\text{C}$ ), was the debonding of the snow crystals when a vacuum was created in the snow layer after the point of the maximum compaction. Gubler (1982) measured the tensile force required to break bonds between ice grains after short contact times (1–500 s), and showed that the bonding of ice crystals is a function of time and temperature with a sharp increase in bonding strength at  $-5^{\circ}\text{C}$ . This short-time bonding is due to the freezing of water in the vicinity of contact points between ice grains created by the increased contact pressure. This bonding effect was neglected during the rapid compaction phase of fresh powder snow since the contact time is very short ( $< 0.1$  s), and thus, the sintering of ice crystals is delayed until maximum compaction is achieved. However, during the rebound of the piston over a relatively longer time period ( $\sim 0.5$  s), the partially sintered fresh powder snow is aerated and an extra damping force due to the debonding of the sintered ice crystals is present. For wind-packed snow, the bonding strength of ice crystals is expected to be very weak during the compaction process ( $\sim 0.7$  s) owing to the low ambient temperature ( $-10^{\circ}\text{C}$ ) (Gubler 1982) and low water content (Colbeck 1997).

The present study should not be confused with the propagation of shockwaves or plastic waves inside snow (Wakahama & Sato 1977; Johnson 1991). For example, Johnson (1991) has developed a simple momentum model to compute the pressure attenuation of a shock wave in snow using prescribed pressure–density curves. This theory is applied to large-amplitude compaction waves following explosions, whose amplitude is several orders of magnitude larger than the excess pore pressure

developed during snowboarding, which is several kPa. Wakahama & Sato (1977) studied the plastic wave propagation inside snow when it is pushed very fast by a moving body, while in the present study the compaction speed is much slower (the maximum velocity of the falling piston is at most a tenth of that in Wakahama & Sato 1977).

Theoretical models to predict the permeability of snow (see summary in Jordan *et al.* 1999) have had only limited success. A principal difficulty is that ice crystals can take on a variety of shapes from planar dendritic (hexagonal) to columnar within each snow classification (Arons & Colbeck 1995). The shape of newly formed snow crystals depends strongly on temperature. Studies of ice crystals in natural clouds (Ono 1970) have shown that there are at least two basic transitions as the temperature is lowered. The primary transition, from plane hexagonal to needle-type columnar, occurs at  $-3.5^{\circ}\text{C}$  and the second transition, from needle or sheath-type columnar back to a stellar or more complex planar dendritic form, occurs at approximately  $-10^{\circ}\text{C}$ . The dimensions of the various ice crystals are summarized in the classic paper by Auer & Veal (1970). Because of the great variety of shapes, ice crystals are often described by a general parameter that is the surface area to mass ratio or specific surface area (SSA) (Fassnacht *et al.* 1999).

There are, however, some semi-empirical or empirical relationships to predict snow permeability. The most widely used formula for relating permeability to crystal size and snow density is the empirical expression of Shimizu (1970):

$$K = 0.077 \exp(-0.0078\rho_s)D^2, \quad (1)$$

where  $D$  is the mean diameter of the snow particles and  $\rho_s$  is the snow density. After scaling the experimental data as a function of the crystal diameter  $D$ , Jordan *et al.* (1999) demonstrated that the porosity dependence of  $K$  follows Shimizu's equation (1) rather closely. In this paper, the Darcy permeability of the undeformed snow sample,  $K_0$ , is obtained from the data of Jordan *et al.* (1999), while its variation with compression follows Shimizu's empirical relationship (1). As shown later in this paper, our predictions for  $K_0$  are very close to those measured by Albert, Shultz & Perron (2000) for similar snow conditions.

We shall present our experimental study in §2, and the theoretical model for the dynamic compression process in §3. In §4, we compare our experimental data and theoretical predictions and interpret the behaviour observed for the two different snow types. Finally, in §5 we conclude by discussing the limitations of the present study and the modifications required to describe human skiing or snowboarding.

## 2. Experiments

### 2.1. Methods

#### 2.1.1. Dynamic compression experiments

In order to obtain critical insights into the behaviour of soft porous media in response to rapid compaction, a new experimental apparatus was designed, fabricated and tested in the field. A schematic of the apparatus is shown in figure 1. It consists of a cylindrical sidewall which is porous and is attached to a solid base plate. A light piston that can carry additional fixed weights can slide freely along the inner surface of the cylindrical porous sidewall and provide a uniform loading to the porous media. The apparatus is designed so that there is no leakage of snow through the porous sidewall or through the clearance gap between the piston and the cylinder. Rigimesh

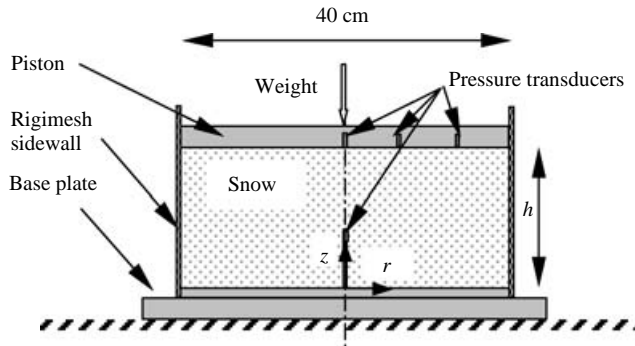


FIGURE 1. Schematic of dynamic snow compression apparatus.

was used to form the desired cylindrical surface, which filtered out all particles with size greater than 0.120 mm. Rigimesh is an arrangement of several screens bonded together for more rigidity. The mesh provides a negligible airflow resistance. This was evident in tests without snow, which indicated no pressure build-up during a free fall of the piston with a weight. This apparatus has not been designed to reproduce realistically the boundary conditions that are encountered in skiing or snowboarding, where the undeformed snow near the edges of the compressed snow layer provides additional resistance, and a permeable snow base is present.

Four high-frequency-response sub-miniature pressure transducers (Kulite Semiconductor Products, model XCS-062-5-D) were installed on the apparatus to measure the time-dependent pore-pressure distribution inside the snow layer and its spatial variation under rapid compression. One transducer was fixed at the centre of the piston; two were installed on the piston at distances  $R/3$  and  $2R/3$  away from the centre, respectively, where  $R$  is the radius of the piston; and the fourth was installed in the snow along the centreline of the cylinder at an adjustable height. The inner diameter of the transducer is 1 mm, which is small enough to ensure good spatial resolution of the local pressure measurement. The pressure transducers were powered by a 9V battery and calibrated in a small portable pressure chamber with controllable pressure. The electrical outputs were filtered and amplified by EC&G pre-amplifiers and signal conditioners and then collected with a data acquisition system of 16 bits resolution (an Iotech Filter 488/8 and an ADC488/8SA). Finally, the signals were transferred to a computer for further processing. Pressure was measured relative to the ambient pressure.

Our instrumented apparatus can not only measure the transient pore pressure response to rapid deformation, but also its spatial variation. The latter is required to address the question of whether the snow beneath the piston is relatively uniformly compressed. This non-uniformity in density can be observed with the pressure distribution measurement along the vertical centreline of our porous cylinder–piston apparatus.

The apparatus was filled with snow up to a height of  $\sim 10$  cm by using a flat-surface snow shovel. Excess snow was removed by using a long sharp steel blade so that a uniform height/depth of snow was reached in all radial positions of the apparatus. The piston was weighted and then released under gravity to compress the snow. The tolerance between the piston and the cylinder wall is large enough to allow the piston to drop with little friction between the sliding surfaces. The air leakage through this narrow gap is negligible compared to the porous sidewall. Setting up

the equipment and apparatus and initial tests lasted several hours. The apparatus worked as expected. No snow leakage was observed through the cylindrical sidewall of the container or through its clearance with piston. The pressure transducers also functioned as expected in the field measurements without problems.

The depth of the snow layer before and after the compression, and its mass were measured to determine the initial and final snow density and porosity.

### 2.1.2. *Static compression experiments*

When the theory in FW was first developed, it was intended to apply to highly compressible porous media in the limit where the structure is so compressible that the normal forces generated by the compression of the solid phase are negligible compared to the pore-pressure forces generated within the porous media. This is never fully achieved in alpine skiing, even for fine-grained wind-packed (less permeable) snow. However, as will be seen later in this paper, at speeds typical of alpine skiing, the duration of contact time of the ski with the snow is so short (less than 0.1 s) that the lift forces generated by the air in the compressed snow layer provide a major component of the ski's support.

In our dynamic compression experiment, the piston is always in contact with snow. As the air inside the snow drains through the porous sidewall, the resistance force of the snow crystals increases until it finally supports the entire load. To gain insight into the mechanical properties of the solid phase in the absence of piston inertia and excess pore pressure, we have measured the quasi-steady force generated when the snow is subject to incrementally increasing compressive forces. The load was added gradually to the piston so that the air in the pores could escape freely without elevating the pore pressure, in contrast to the dynamic experiments in which the air in the pores is temporarily trapped before it escapes. This has also made it possible to separate out the inertial effect associated with the acceleration and deceleration of the piston. The time interval between the load increments is long enough to allow air to escape ( $> 1$  s), but short enough to avoid bonding of the snow crystals until the final deformation is achieved and the motion is arrested. The apparatus described in the previous section for the dynamic crushing of porous media was used to determine the relation between applied quasi-static stress and displacement. This will enable us to obtain realistic estimates of the stress that is applied by the solid phase as the compression proceeds. The deformation of the snow sample was measured immediately after load application. Thus, creep deformation was excluded.

## 2.2. *Snow sample characterization*

The experiments were carried out in March 2002 and 2003 at Hunter Mountain in upstate NY, near the village of Tannersville. Two different types of snow sample were tested.

### 2.2.1. *Wind-packed snow*

Natural snow, two days old, was used in the March 2002 experiments. It was fine-grained, wind-packed snow. This could be attributed to the low temperature ( $-10^{\circ}\text{C}$ ), the windy weather condition, and the deposition of snow. The ice crystals took a needle-type shape typical of low-temperature wind-deposited snow. The snow sample had a relatively low porosity ( $\phi_0 = 0.6$ ) and Darcy permeability, similar to that shown in figure 6 of Jordan *et al.* (1999).

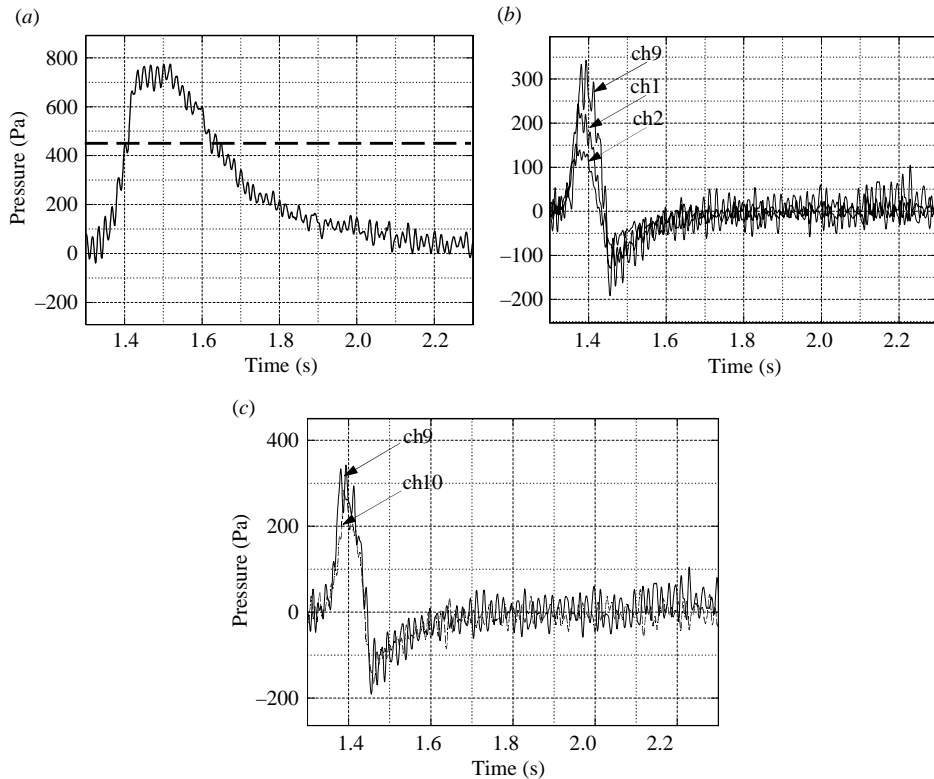


FIGURE 2. Time-dependent pressure signals obtained from the dynamic compression experiments, (a) wind-packed snow, load = 5.9 kg, equivalent to an average normal stress of 456.6 Pa,  $h_0 = 11.43$  cm,  $h_f/h_0 = 0.78$ ,  $P_{max} = 744$  Pa, signals are from the central pressure transducer on the piston; (b) fresh snow,  $h_0 = 8.29$  cm,  $h_f/h_0 = 0.83$ , load = 10 kg, equivalent to an average normal stress of 778.2 Pa, signals are from the three equally spaced pressure transducers on the piston, ch9 refers to the pressure transducer at the centre of the piston, ch1 and ch2 refer to the pressure transducers on the piston at distances  $R/3$  and  $2R/3$  away from the centre, respectively, where  $R$  is the radius of the piston; (c) fresh snow,  $h_0 = 8.29$  cm,  $h_f/h_0 = 0.83$ , load = 10 kg, signals are from the pressure transducers along the centreline of the cylinder where ch10 is the pressure transducer mounted along the centreline 4.25 cm above the base of the cylinder.

### 2.2.2. Fresh snow

The most recent experiments were carried out in March 2003 at the same location as the experiments in the previous year. Natural freshly fallen snow was used in these experiments. The weather conditions were mild and breezy, and the ambient temperature was  $-4^\circ\text{C}$ . The snow was quite soft and fluffy and the ice crystals had a typical hexagonal shape. The fresh snow is characterized by relatively high porosity ( $\phi_0 = 0.8$ ) and Darcy permeability, similar to that shown in figure 6 of Jordan *et al.* (1999).

## 2.3. Experimental results

### 2.3.1. Dynamic compression experiments

#### Wind-packed snow

Six dynamic compression experiments were performed with wind-packed snow. Figure 2(a) shows a representative time-dependent trace of the pressure signals at the centre of the piston during the dynamic compression process using a piston mass

of 5.9 kg. This is equivalent to an average normal stress of 456.6 Pa applied on the bottom surface of the piston. As can be seen from this figure, the pore pressure inside the snow powder becomes greater than the applied normal stress very quickly. This clearly indicates that air is transiently trapped before it escapes as the theory in FW suggests. The compression ratio,  $\Delta h/h_0$ , in this experiment was  $=0.22$ , with initial height  $h_0 = 11.43$  cm. The pore air pressure rises rapidly, reaches its maximum value of 744 Pa at the centre of the piston within about 0.15 s and then falls back to zero within 1 s. At the end of the experiment, the applied normal force is supported by the normal stress in the solid phase at its new equilibrium, and the porosity of the snow sample after compaction is 0.47.

The time scale of compression is in the same range as the characteristic time of skiing (0.05 to 0.2 s) if we assume a ski or snowboard length between 1.6 m and 2 m and a downhill speed between  $10 \text{ m s}^{-1}$  and  $30 \text{ m s}^{-1}$ . This initial experiment was performed on the first design of the apparatus in which there was only a single central pressure transducer.

### *Fresh snow*

Twelve dynamic snow compression experiments with fresh snow were performed with a load of 10 kg, which is equivalent to an average normal stress of 778.2 Pa applied on the bottom surface of the piston. The signals were further processed off line by using a digital Butterworth low-pass filter design. Figures 2(b) and 2(c) show the time-dependent pressure signals during a representative test. In figure 2(b), signals obtained from the three equally spaced pressure transducers on the piston are shown, where ch9 refers to the pressure transducer at the centre of the piston, ch1 and ch2 refer to the pressure transducers on the piston at distances  $R/3$  and  $2R/3$  away from the centre, respectively. Figure 2(c) shows signals obtained from the pressure transducers along the centreline of the cylinder, where ch10 is the pressure transducer mounted along the centreline, 4.25 cm above the base of the cylinder. The transducers ch9, ch1 and ch2 capture the radial pressure distribution, while ch9 and ch10 describe the pressure distribution vertically.

As shown in figures 2(b) and 2(c), the pore pressure builds to its peak value within  $\sim 0.1$  s, and then relaxes on a time scale ( $\sim 0.1$  s) that is significantly shorter than the wind-packed snow experiment ( $\sim 1$  s). The peak value of pressure at the center of the piston was 300 Pa, roughly 45 % of the average normal pressure applied on the bottom surface of the piston. There is no extended pressure relaxation phase for the fresh snow because the dimensions of the piston are too small and the value of  $K$  too large for the excess pore pressure to support the full piston weight. We can also see that a sub-atmospheric vacuum pressure is created before the pore pressure finally returns to atmospheric pressure. In this experiment, the compression ratio,  $\Delta h/h_0 = 0.17$  and  $h_0 = 8.29$  cm. The initial porosity was 0.8, which is typical for fresh snow (Jordan *et al.* 1999).

### 2.3.2. *Static compression experiments*

Static experiments were performed on the same types of snow sample using the same apparatus immediately following the dynamic compression experiment in the field. We observed that a small load increment ( $\sim 0.5$  kg) would not compress the snow sample, whereas, a medium increment ( $\sim 2$  kg) could. This is because the bonding between the snow crystals creates a threshold for the resistance to compression.

Figure 3 shows a typical incremental loading curve sequence for a static compression test on natural fresh snow with an initial porosity of 0.8. Both the applied load  $F$

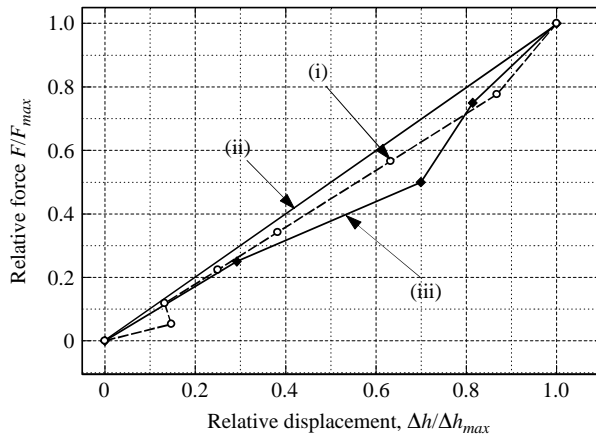


FIGURE 3. Force/displacement relation obtained in the quasi-static compression experiment with snow. (i) Yong & Fukue (1977, figure 7). (ii) Linear behaviour. (iii) Static compression experiment.

and the displacement  $\Delta h$  have been non-dimensionalized by their corresponding maximum values. The data for the incremental loading experiments in Yong & Fukue (1977) on natural medium-coarse-grained snow with an initial porosity of 0.6 are also plotted for comparison. They were obtained by applying loads incrementally to a snow sample under drained conditions, over a period of two and a half minutes, until a final load intensity of  $0.5 \text{ kg cm}^{-2}$  was reached. As can be seen from this figure, the current static experimental results are similar to the Yong & Fukue data.

The results in figure 3 indicate that the supporting force from the solid phase of the snow sample increases with increasing deformation. This is because the intergranular contacts of the snow crystals become increasingly greater following the initial instantaneous compression. In our porous cylinder–piston experiments, with either wind-packed snow (load = 5.9 kg) or fresh snow (load = 10 kg), the maximum surface displacements were  $< 22\%$  of the undeformed height of the snow layer. This is considerably less than the deformation that would be achieved for large applied loads on our low-density snow where the maximum density could be as high as  $0.875 \text{ g cm}^{-3}$ . This experimentally determined force–displacement profile was used to estimate the increasing force that the solid snow phase would exert on the falling piston during the dynamic snow compression experiments. This force will be used in our theoretical model to predict the time-dependent evolution of pore pressure.

### 3. Theoretical model

In this section, we develop a theoretical model to predict the pore pressure distribution during the dynamic compression of snow. The motion of the falling piston is modelled by applying Newton's law. As shown in figure 1, the piston is released from rest and starts falling toward a solid planar surface. The distance between the piston and the ground is assumed to be uniform in the radial direction so that the displacement,  $\Delta h$ , is independent of  $r$  and varies only with time. Balance of forces acting on the piston requires that

$$m \frac{d^2 h}{dt^2} = -mg + F_{air} + F_{snow}, \quad (2)$$

where  $m$  is the mass of the piston,  $F_{air}$  is the integral of the dynamic pore pressure on the piston and  $F_{snow}$  is the resistance force due to the solid phase, the snow's intergranular contact. This model is similar to Terzaghi's (1943) consolidation theory, which has been applied in both soil mechanics and biomechanics to describe the decay of pore pressure in porous media. An approximation for  $F_{snow}$  was obtained from the static compression experiment described in the previous section, where the porous media is compressed slowly so that the trapped air has enough time to escape and the entire load is supported by the solid phase. The resistance-deformation relation in figure 3 can be written in the form:

$$\frac{F_{snow}}{F_{max}} = f\left(\frac{\Delta h}{\Delta h_{max}}\right). \quad (3)$$

The dynamic pore pressure force  $F_{air}(t)$  is obtained by integrating the time-dependent pressure acting over the piston:

$$F_{air}(t) = \int_0^R 2\pi r P(r, h, t) dr, \quad (4)$$

where  $R$  is the radius of the cylinder, and  $P(r, h, t)$  is determined by solving for the instantaneous pore pressure distribution inside the snow sample.

The flow in this device is time-dependent, but the instantaneous flow is approximately described by a quasi-steady axisymmetric flow within the cylinder which satisfies Darcy's law:

$$\mathbf{q} = -\frac{K}{\mu} \nabla P, \quad (5)$$

where  $\mu$  is the fluid viscosity,  $K$  is the Darcy permeability,  $\mathbf{q}$  is the specific flux vector with components  $q_r, q_\theta, q_z$  in the cylindrical coordinates  $(r, \theta, z)$ . In a consolidating porous medium, where the porous matrix undergoes deformation during the process of transient fluid flow,  $\mathbf{q}$  is the relative specific flux with respect to the solid grains. In the present application, the displacement of the solid particle is less than 22% of the  $\sim 10$  cm thickness of the snow layer. In contrast, the characteristic discharge distance for the air is equal to the radius of the cylinder, which is 20 cm. As a result, the ice crystal velocity is negligible compared to the air velocity and  $\mathbf{q}$  is approximated by the absolute flux with respect to a fixed coordinate system. Thus, we take

$$\mathbf{q} = \phi \mathbf{V}_l, \quad (6)$$

where  $\mathbf{V}_l$  is the local absolute velocity vector (velocity of air within the pores) and  $\phi$  is the porosity,

$$\phi = U_v / U_i, \quad (7)$$

where  $U_i$  is the volume of the porous medium, and  $U_v$  is the volume of void space within  $U_i$ . Equation (6) is sometimes called the Dupuit–Forchheimer's equation (Bear 1972). If the snow layer is assumed to be homogenous with a thickness  $h$  at any time  $t$ , and initially  $h = h_0$ ,  $\phi = \phi_0$ , we obtain from (7)

$$\phi = 1 - \frac{h_0}{h}(1 - \phi_0). \quad (8)$$

From continuity we require that

$$\nabla \cdot (\rho \mathbf{q}) + \frac{\partial(\rho \phi)}{\partial t} = 0, \quad (9)$$

where  $\rho$  is the density of the air. Equation (9) describes the transient deformation of a consolidating medium. In our dynamic compression experiments, the pressure under the piston never exceeds 3 kPa above ambient pressure. Thus, the pressure change with respect to ambient pressure is only about 3 %, the Mach number is  $\ll 1$ , and thus the air can be treated as incompressible. In fact, the isothermal compressibility is of the order of  $10^{-4} \text{ Pa}^{-1}$  in the current application. Equation (9) then reduces to

$$\nabla \cdot \mathbf{q} + \frac{\partial \phi}{\partial t} = 0. \tag{10}$$

From (5) and (10), we obtain

$$\nabla^2 P - \frac{\mu}{K} \frac{\partial \phi}{\partial t} = 0. \tag{11}$$

After substituting for  $\phi$  by using (8), we can write (11) in axisymmetric cylindrical coordinates as

$$\frac{1}{r} \frac{\partial}{\partial r} \left( r \frac{\partial P}{\partial r} \right) + \frac{\partial^2 P}{\partial z^2} + \frac{\mu}{K} \frac{h_0(\phi_0 - 1)}{h^2} \frac{dh}{dt} = 0. \tag{12}$$

Using quasi-static and homogeneous assumptions, we find that the source term, corresponding to the last term on the left-hand side of (12) is a function of time only.

It is desirable to introduce new dimensionless variables,  $P'$ ,  $r'$ ,  $z'$ ,  $h'$  and  $t'$ , as follows:

$$P' = \frac{P}{P_c}, \quad r' = \frac{r}{R}, \quad z' = \frac{z}{h_0}, \quad h' = \frac{h}{h_0}, \quad t' = \frac{t}{t_c}, \tag{13a-d}$$

where

$$t_c = \frac{\mu R^2(\phi_0 - 1)}{P_c K}, \quad P_c = \frac{mg}{\pi R^2}. \tag{13e,f}$$

Substituting (13) into (12), we obtain a dimensionless equation for  $P'(r', z', t')$ :

$$\frac{1}{r'} \frac{\partial}{\partial r'} \left( r' \frac{\partial P'}{\partial r'} \right) + 4\beta^2 \frac{\partial^2 P'}{\partial z'^2} + \frac{1}{h'^2} \frac{dh'}{dt'} = 0, \tag{14}$$

where  $\beta = R/2h_0$ .

At the base planar boundary,  $z = 0$ , the no-penetration condition requires that

$$q|_{z=0} = 0 \Rightarrow \left. \frac{\partial P'}{\partial z'} \right|_{z'=0} = 0. \tag{15a}$$

At  $z = h(t)$ , the lower surface of the piston, the no-penetration condition requires that the flow have a uniform downward average velocity  $dh/dt$ :

$$q|_{z=h} = \frac{dh}{dt} = -\frac{K}{\mu} \frac{\partial P}{\partial z} \Rightarrow \left. \frac{\partial P'}{\partial z'} \right|_{z'=h'} = -\frac{1}{4\beta^2(\phi_0 - 1)} \frac{dh'}{dt'}. \tag{15b}$$

Because of the symmetry of the flow with respect to the  $z$ -axis and the nature of the pressure boundary conditions, it is evident that

$$\left. \frac{\partial P'}{\partial r'} \right|_{r'=0} = 0, \tag{15c}$$

$$P'|_{r'=1} = 0. \tag{15d}$$

The boundary-value problem (14)–(15) for the quasi-static pressure distribution inside the snow layer depends on two parameters,  $\beta$  and  $\phi_0$ , and has the solution:

$$P'(r', z', t') = \sum_{k=1}^{\infty} a_k J_0(\lambda_k r') \cosh \frac{\lambda_k z'}{2\beta} + \frac{1}{4h'^2} \frac{dh'}{dt'} (1 - r'^2), \tag{16}$$

where

$$a_k = \frac{-\frac{1}{2\beta(\phi_0 - 1)} \frac{dh'}{dt'} \int_0^1 r' J_0(\lambda_k r') dr'}{\lambda_k \sinh\left(\frac{\lambda_k}{2\beta} h'\right) \int_0^1 r' J_0^2(\lambda_k r') dr'}, \tag{17}$$

and

$$J_0(\lambda_k) = 0. \tag{18}$$

Applying (13) in (4), we rewrite the dynamic pore pressure force  $F_{air}(t)$  acting on the piston in dimensionless form:

$$F'_{air}(t') = \frac{F_{air}(t)}{mg} = 2 \int_0^1 P'(r', h', t') r' dr', \tag{19}$$

Substituting (16) into (19),  $F'_{air}(t')$  is given by

$$F'_{air}(t') = \left\{ -\frac{1}{\beta(\phi_0 - 1)} \sum_{k=1}^{\infty} \frac{\left[ \int_0^1 r J_0(\lambda_k r') dr' \right]^2}{\lambda_k \int_0^1 r' J_0^2(\lambda_k r') dr'} \coth\left(\frac{\lambda_k}{2\beta} h'\right) + \frac{1}{8h'^2} \right\} \frac{dh'}{dt'}. \tag{20}$$

In (13e), the Darcy permeability  $K$  of the snow sample is also a function of compression. We employ Shimizu’s equation given by (1) to predict this relationship (Shimizu 1970). During the compression process, the density of the snow layer changes owing to the motion of the upper boundary. For a snow layer with an initial uniform density,  $\rho_{s0}$ , the deformation-dependent average snow density,  $\rho_s(h)$ , is expressed as

$$\frac{\rho_s(h)}{\rho_{s0}} = \frac{h_0}{h}. \tag{21}$$

If the mean diameter of the ice crystal,  $D$ , remains the same, and the Darcy permeability of the undeformed snow is  $K_0$ , we obtain from (1) and (21),

$$K = 0.077 \exp \left[ \frac{h_0}{h} \ln \frac{K_0}{0.077 D^2} \right] D^2. \tag{22}$$

Employing dimensionless variables (13), we substitute (3), (19) and (20) back into (2), and obtain

$$\gamma \frac{d^2 h'}{dt'^2} - \left\{ -\frac{1}{\beta(\phi_0 - 1)} \sum_{k=1}^{\infty} \frac{\left[ \int_0^1 r J_0(\lambda_k r') dr' \right]^2}{\lambda_k \int_0^1 r' J_0^2(\lambda_k r') dr'} \coth\left(\frac{\lambda_k}{2\beta} h'\right) + \frac{1}{8h'^2} \right\} \frac{dh'}{dt'} - f \left( \frac{1 - h'}{1 - h'_f} \right) + 1 = 0, \tag{23}$$

where  $\gamma = (t_g/t_c)^2$ ,  $t_g = \sqrt{h_0/g}$  and  $h_f$  is the final position of the piston.  $\gamma$  is the square of the ratio of two time scales, the gravitational time scale  $t_g$  and the viscous draining time scale  $t_c$ . Since  $\gamma$  is very small, we anticipate that the leading term in (23) is important at very short times and after that the movement of the piston is governed by the remaining terms on the right-hand side of (3). This is a singular perturbation problem in which a small parameter multiplies the highest-order derivative term. At  $t=0$ ,

$$h' \Big|_{t'=0} = 1, \quad \frac{dh'}{dt'} \Big|_{t'=0} = 0. \quad (24a, b)$$

The differential equation (23) was solved numerically subject to the initial conditions given by (24a, b). Once  $h'(t)$  was obtained, the pore pressure distribution was found by substituting our numerical result for  $h'(t)$  into (16).

## 4. Results and discussions

### 4.1. Wind-packed snow

For the wind-packed snow sample, the initial porosity  $\phi_0$  was 0.6, the initial thickness,  $h_0$ , of the snow layer before compaction was 11.43 cm, and the final thickness,  $h_f$ , after compaction was  $0.78h_0$ . The applied load was 5.9 kg, the mean diameter of the ice crystal,  $D$ , was estimated to be 0.42 mm based on the measurements in Jordan *et al.* (1999). For solid-volume fractions  $> 0.2$ , the dynamic viscosity,  $\mu$ , of the trapped air inside the snow, is not simply the air viscosity at the same temperature. However, it is reasonable to assume that  $\mu$  is unchanged in the experiment with a value  $\mu = 1.667 \times 10^{-5} \text{ N s m}^{-2}$ , while  $K$  varies with compression. Using these parameter values in (23), we obtain the time-dependent displacement and velocity of the piston for different values of initial Darcy permeability  $K_0$ . The results are plotted in figures 4(a) and 4(b), respectively. The initial values of  $K_0$  are varied between  $0.25 \times 10^{-9} \text{ m}^2$  and  $1.0 \times 10^{-9} \text{ m}^2$ , which are typical values for wind-packed snow (Jordan *et al.* 1999; Albert *et al.* 2000, 2002; Albert & Shultz 2002). The inverse of  $K$  is a measure of the resistance that the air encounters as it flows through the porous media, or equivalently, the damping force of the trapped air that acts on the piston. We expect that as  $K_0$  decreases it will take longer for the air to escape since it encounters an increased resistance. Thus, the velocity of the falling piston decreases owing to the increased air damping force. As can be seen from figure 4, our theoretical prediction for the motion of the piston captures these features.

We have computed the time-dependent pore pressure  $P/P_{max}$  at the location of the central pressure transducer on the underside of the piston after it is released from rest for different values of permeability  $K_0$  and have compared these predictions with our experimental data, as shown in figure 5. The solid curves in this figure are our theoretical model predictions for the time-dependent decay of the excess pore pressure. The pressure relaxation time is seen to increase as  $K_0$  decreases. The curve that provides the best fit to the experimental data corresponds to an initial Darcy permeability,  $K_0$ , of  $5.0 \times 10^{-10} \text{ m}^2$ . Although the choice of  $K_0$  varies substantially with the snow sample, this value of  $K_0$  is typical of the measurements in wind-packed fine snow (Jordan *et al.* 1999; Albert *et al.* 2000; 2002; Albert & Shultz 2002). For example, the measurements by Albert *et al.* (2000) for wind-blown snow in the top 0–20 cm indicate a  $K_0$  of 5 to  $9 \times 10^{-10} \text{ m}^2$ , whereas our best fit in figure 5 indicates  $K_0$  between 5 and  $7.5 \times 10^{-10} \text{ m}^2$  for similar snow conditions, which is very close.

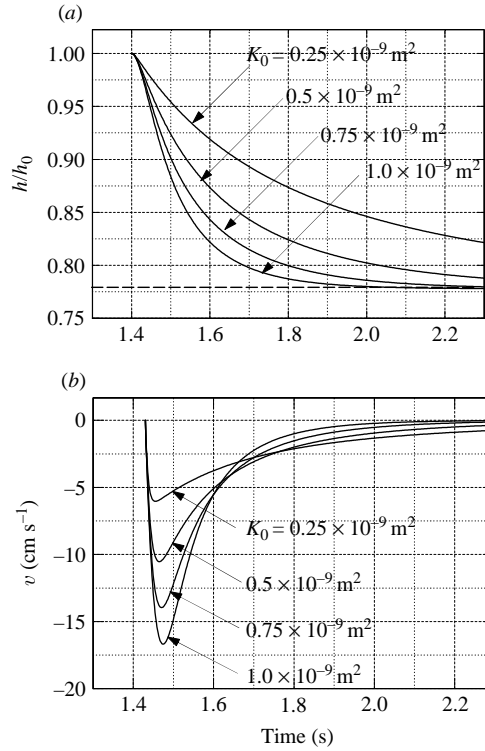


FIGURE 4. Theoretical predictions for the time-dependent (a) displacement  $h/h_0$  and (b) velocity of the piston for different values of initial Darcy permeability  $K_0$  of wind-packed snow, where the initial thickness of the snow layer,  $h_0 = 11.43$  cm, the initial snow porosity,  $\phi_0 = 0.6$ . The dashed line in (a) denotes the measured thickness of the snow layer after the compaction,  $h_f/h_0 = 0.78$ .

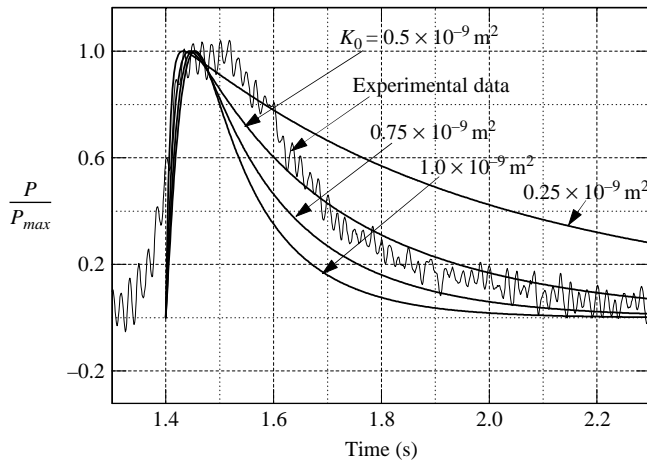


FIGURE 5. Comparison between the theoretical predictions of the time-dependent pressure and the experimental data for various values of the initial Darcy permeability  $K_0$ . The test sample was wind-packed snow with initial thickness,  $h_0 = 11.43$  cm,  $h_f/h_0 = 0.78$ , applied mass  $m = 5.9$  kg,  $P_{max} = 744$  Pa.

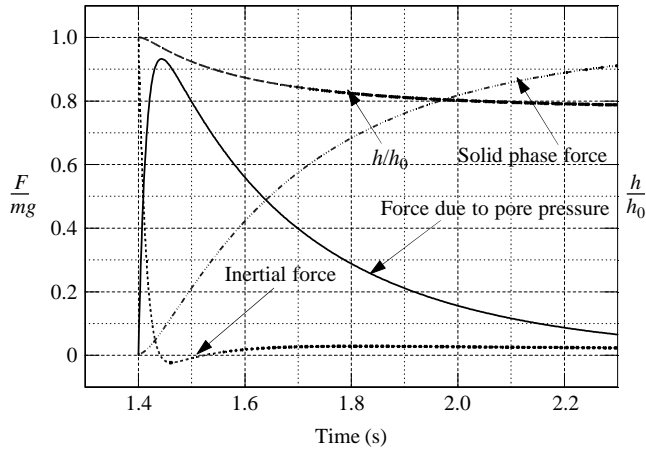


FIGURE 6. Time-dependent forces during dynamic compression of wind-packed snow.

We observed a rapid rise in pore pressure and then a decay that occurs on a time scale of roughly 0.7 s (see figure 5). In contrast, the length of time that a 1.5 m snowboard travelling at  $15 \text{ m s}^{-1}$  would be in contact with a given patch of snow would be 0.1 s. It is clear from the figure that after 0.1 s, the excess pore pressure has only started to relax. We expect that much of the weight of the snowboarder would be supported by the air that is still trapped in the partially compressed snow layer.

These dynamic compression experiments in wind-packed snow demonstrate that a sudden compression of wind-packed snow with limited porosity can generate peak pore pressures which are substantially larger than the average applied normal stress (see figure 2a). The lumped parameter model based on the consolidation theory developed herein can reproduce the major features of the experimental data. The theoretical model provides further insight into the relative importance of the individual forces during the compression process. This is summarized in figure 6 which shows the time variation of the three forces that appear in (2) normalized by the applied weight,  $mg$ . The summation of all normalized forces at any time must equal unity. In the initial stages of the compression, the force due to the pore pressure builds up very quickly and is counterbalanced nearly entirely by the inertial force of the piston. Close to  $P_{max}$ , the piston achieves its maximum downward velocity, the inertial force vanishes and the solid phase force starts to increase. As noted earlier in (23), the highest derivative term which describes the inertia, is multiplied by a small parameter  $\gamma$ . This term is only important for short times of order  $\sqrt{\gamma}t_c$ . The solid phase force continues to increase until it fully supports the piston weight when the air pore pressure is completely vented. The good agreement between the measured and predicted pore pressure relaxation in figure 5 would not have been possible if the experimentally measured relation, given by (3), for the force exerted by the solid phase were not reasonably accurate.

It is evident from figure 6 that at  $t = 1.5$  s, the snow has been compressed up to only  $\sim 40\%$  of its final deformation. At this point, the pore pressure supplies more than 80% of the total lift, the solid phase about 20% and the inertial force is negligible. Although the present experiments do not realistically reproduce the boundary conditions that are encountered in skiing or snowboarding, the contact time of a 1.5 m snowboard moving at  $15 \text{ m s}^{-1}$  with the snow layer underneath, is in the range where the pore pressure is the dominant lifting force. The time scales for

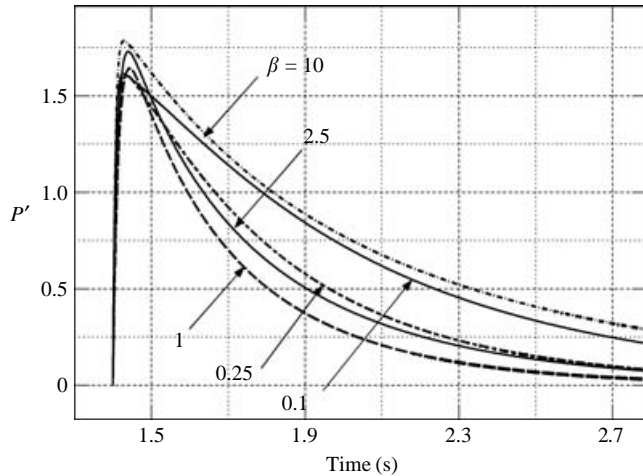


FIGURE 7. Theoretical predictions for the time-dependent pressure distribution,  $P'$ , at the centre of the piston for different values of  $\beta$ , where  $h_f/h_0 = 0.78$ ,  $K_0 = 5.0 \times 10^{-10} \text{ m}^2$ .

the motion of the piston in these experiments are more representative of a snowboard than a ski because of the piston dimensions. For skis, the relaxation time will be significantly shorter since its narrow width will allow trapped air to escape laterally. Consequently, the solid phase is expected to carry a substantially greater portion of the load under a ski than under a snowboard.

From (14), we find that the pressure relaxation in the porous cylinder–piston device depends on the parameter,  $\beta = R/2h_0$ .  $\beta$  denotes the weight-bearing area to ventilation-perimeter-area ratio. In figure 7, we plot the theoretical predictions for the time-dependent pressure distribution,  $P'$ , at the centre of the piston for different values of  $\beta$ , where  $h_f/h_0 = 0.78$ ,  $K_0 = 5.0 \times 10^{-10} \text{ m}^2$ . It can be seen from this figure, for  $\beta > 1$ , increase of  $\beta$  will increase the peak value of pressure and lengthen the pressure relaxation time. This is because the ventilation area is too small and the trapped air cannot escape easily. However, it is also observed in this figure that for  $\beta < 1$ , increase in  $\beta$  will decrease the duration of pore pressure relaxation. This is because for  $\beta \ll 1$ , the air only vents in the vicinity of the piston and the full height of the snow column does not contribute to the drainage of the air. Thus, we have a different venting behaviour in either the small or large  $\beta$  limit with a transition that occurs at roughly  $\beta = 1$ .

#### 4.2. Fresh snow

For the fresh snow sample, the initial porosity,  $\phi_0$ , was 0.8, the thickness,  $h_0$ , of the snow layer before compaction was 8.29 cm, and the final thickness,  $h_f$ , after compaction was  $0.83h_0$ . The applied mass was 10 kg. Using the data in figure 6 of Jordan *et al.* (1999), we estimated the mean diameter,  $D$ , of the ice crystal to be 1 mm, and the undeformed Darcy permeability,  $K_0$ , to be  $\sim 10^{-8} \text{ m}^2$  for this sample. The solid fraction,  $(1-\phi_0)$ , was 0.2. Since fresh snow is more porous and its Darcy permeability is 20–30 times greater than wind-packed snow, we expect that the piston will be poorly damped by the trapped air in its downward descent, as noted in figures 2(b) and 2(c). The peak value of pressure at the centre of the piston during the compaction process is only about 45% of the average normal pressure applied on the bottom surface of the piston, and vacuum pressure is created before the pore pressure finally returns to atmospheric level, indicating a rebound of the piston.

It is widely recognized that snow is a collection of ice grains interconnected in an intricate three-dimensional structure. The grain bonds between sintered snow crystals play an important role in determining the mechanical properties of snow, which are structure- and time-dependent at a given temperature. During the rapid compression, the bonds between the snow grains are broken abruptly and we would not expect a significant damping effect from the snow crystals. The constitutive equation (3) obtained from the static experiment has no memory effect and predicts the resistance force from the snow sample closely. However, as the piston rebounds over a relatively longer time period after its maximum compression, the partially sintered snow sample is aerated and experiences an expansion process, during which the relative motion between the ice grains has to overcome this aeration effect and an additional damping force from the debonding of the sintered snow crystals. Gubler (1982) measured single ice contact bond growths between the tips of ice cones that resulted in fracture (debonding). They showed that the tensile force during fracture scaled linearly with the compression force during bond formation and that a tensile force of up to 0.15 N could be produced after 1 s compression at an ambient temperature of  $T = -0.1^\circ\text{C}$  for a compression force of  $10^{-2}$  N. If we multiply this effect by many grains, we expect that the damping force due to debonding of ice crystals is linearly proportional to velocity since this is the rate at which bonds are being broken. Thus, we approximate this debonding force by  $\eta(dh/dt)$  mg, where  $\eta$ , the debonding coefficient, is determined by requiring that the theoretical prediction for the piston rebound process fits our experimental data once  $K_0$  is determined from the downward phase of the piston motion. During the rebound, this damping effect from the solid phase is much greater than that of the trapped air due to the much slower velocity of the piston.

Based on the above analysis, we divide the dynamic compression process and its rebound into two consecutive motions. First, a compression ending at  $\Delta h_{max}$  and second, a rebound to the final equilibrium position. For the compression phase, the only unknown parameter is the value of the initial Darcy permeability  $K_0$ , and for the rebound phase, the only unknown is the snow damping parameter  $\eta$ .

Figure 8 shows the time-dependent pressure  $P$  at the centre of the piston for different values of initial Darcy permeability  $K_0$  for the compression phase, and its comparison with the experimental data (ch9 in figure 2). These values of  $K_0$  are typical for fresh snow (Jordan *et al.* 1999). Since  $1/K$  reflects the distributed Darcy resistance of the solid as the air flows through, it is expected that the pore pressure will decrease as  $K_0$  increases. We note from this figure that  $K_0 = 1.7 \times 10^{-8} \text{ m}^2$  provides a best fit to the experimental data. As can be seen from the figure, the pressure relaxation time for fresh snow ( $\sim 0.1$  s) is significantly shorter than that for the wind-packed snow ( $\sim 0.7$  s), since the former has much higher  $K_0$  ( $1.7 \times 10^{-8} \text{ m}^2$ ) and lower solid fraction (0.2). The rapid descent during the compaction phase does not allow for sintering of ice crystals until maximum compaction is achieved.

The theoretical predictions for the time-dependent displacement and velocity of the piston before the start of the rebound are plotted in figures 9(a) and 9(b), respectively, for the same values of  $K_0$  as in figure 8. We observe the same behaviour as for wind-packed snow, i.e. the higher the initial permeability, the less the aerodynamic damping and the larger the value of  $\Delta h_{max}$ .

During the rebound,  $K_0 = 1.7 \times 10^{-8} \text{ m}^2$ , and the dependence of  $K$  on deformation follows Shimizu's relationship, given by (1). The only unknown parameter is the debonding coefficient,  $\eta$ . Figure 10 shows the theoretical predictions for the time-dependent pressure at the centre of the piston (ch9 in figure 2) for different values of  $\eta$  and their comparison with the experimental data. We observe in this figure that

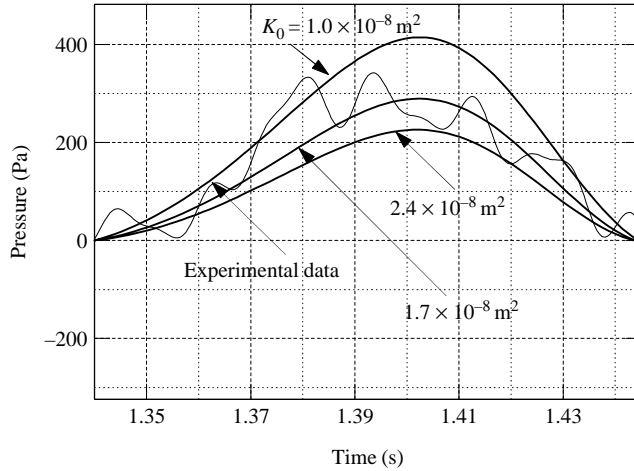


FIGURE 8. Theoretical predictions for the time-dependent pressure at the centre of the piston and their comparison with the dynamic experimental data. The initial values of snow permeability,  $K_0$  are  $1.0 \times 10^{-8} \text{ m}^2$ ,  $1.7 \times 10^{-8} \text{ m}^2$  and  $2.4 \times 10^{-8} \text{ m}^2$ , respectively. The initial porosity  $\phi_0 = 0.8$ , the initial thickness  $h_0 = 8.29 \text{ cm}$ ,  $h_f/h_0 = 0.83$ , load = 10 kg.

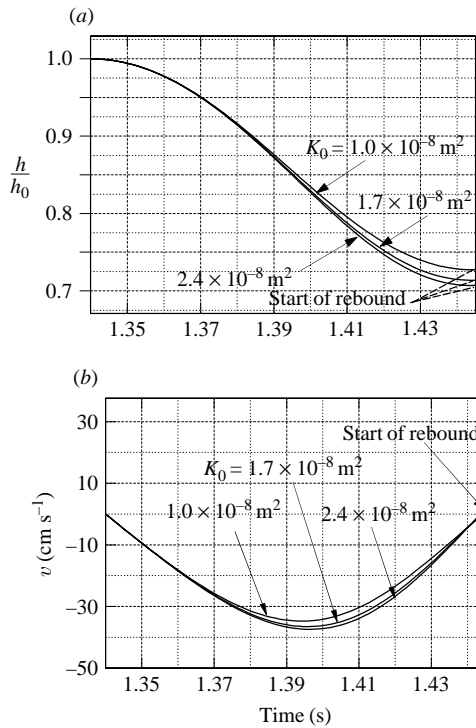


FIGURE 9. Theoretical predictions for the time-dependent (a) displacement and (b) velocity of the piston before the start of the rebound, which reveals the dependence of the piston motion on different values of the initial Darcy permeability  $K_0$  during the dynamic compression with fresh snow. The initial porosity  $\phi_0 = 0.8$ , the initial thickness  $h_0 = 8.29 \text{ cm}$ ,  $h_f/h_0 = 0.83$ , load = 10 kg.

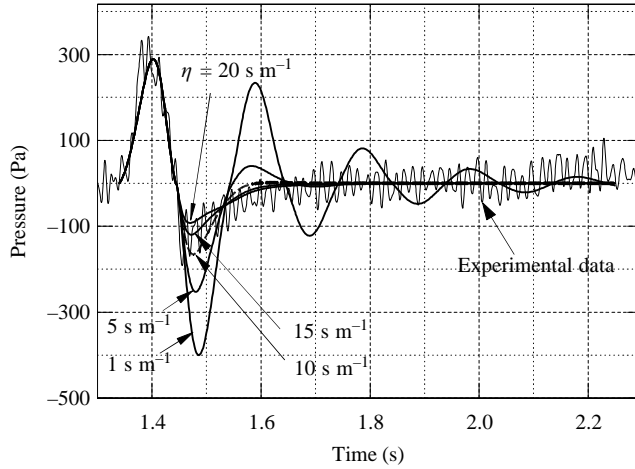


FIGURE 10. Theoretical predictions for the time-dependent pressure at the centre of the piston and their comparison with the dynamic experimental data for fresh snow. The initial values of snow permeability,  $K_0 = 1.7 \times 10^{-8} \text{ m}^2$  and the debonding coefficient  $\eta$  were chosen as  $\eta = 1, 5, 10, 15$  and  $20 \text{ s m}^{-1}$ , respectively. The initial porosity  $\phi_0 = 0.8$ , the initial thickness  $h_0 = 8.29 \text{ cm}$ ,  $h_f/h_0 = 0.83$ , load = 10 kg.

for small values of  $\eta$  (e.g.  $\eta = 1 \text{ s m}^{-1}$ ), the damping force is insufficient to dissipate the inertia of the piston and the theory predicts oscillations; for large values of  $\eta$  (e.g.  $\eta = 20 \text{ s m}^{-1}$ ), the damping force from the debonding of the snow crystals is too large and the theoretical predictions for the pore air pressure are higher than the experimental data. The value of  $\eta$  that provides a best fit to the experimental data is  $\eta = 15 \text{ s m}^{-1}$ .

Figures 11(a) and (b) show the theoretical predictions for the time-dependent displacement and velocity of the piston for the same values of  $\eta$  as in figure 10. From these figures we conclude that for small values of  $\eta$ , oscillations are predicted due to insufficient damping, whereas for large values of  $\eta$ , the increased debonding force significantly decelerates the piston and increases its rebound time.

We next examine the pressure distribution in the radial direction beneath the piston surface. These results are plotted in figure 12, where the theoretical prediction is compared with the experimental data at  $t = 1.40 \text{ s}$ , when the peak pressure is achieved. As can be seen from this figure, the theoretical results for  $K_0 = 1.7 \times 10^{-8} \text{ m}^2$  and  $\phi_0 = 0.8$  show excellent agreement with the experimental data, and the pressure distribution in the  $r$ -direction is very close to parabolic. This is not surprising since the pressure gradient in the radial direction is dominant, and a simple plug-flow model would predict a parabolic pressure distribution in this direction.

The pressure distribution along the centreline of the cylinder (not shown here) was also computed at  $t = 1.40 \text{ s}$ , when the peak value of pressure is achieved. This indicates that the pressure gradient in the  $z$ -direction is quite small. This result is not unexpected since the air can only escape in the  $r$ -direction where the pressure drop is much larger. The theoretical prediction for the peak value of pressure at  $z = 4.25 \text{ cm}$  is 276 Pa, very close to the experimental value (280 Pa) at the same position. The small pressure difference along the centreline of the cylinder also negates the possibility of non-uniform compression and the pressure-wave propagation on the time scale of interest.

Figure 13 shows the time-dependent variation of the scaled inertial, pore-pressure, solid phase and debonding forces for the compression of fresh snow. In contrast to

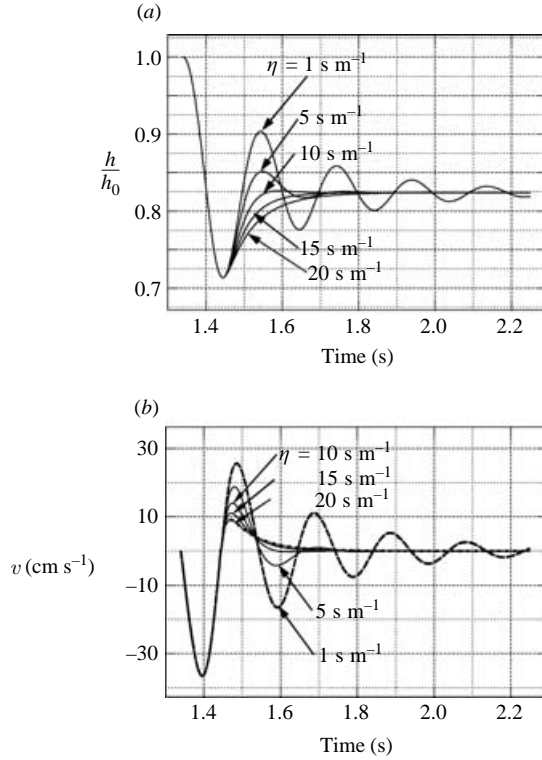


FIGURE 11. Theoretical predictions for the time-dependent (a) displacement and (b) velocity of the piston for different values of debonding coefficient  $\eta$  when the initial Darcy permeability  $K_0 = 1.7 \times 10^{-8} \text{ m}^2$ , the initial porosity  $\phi_0 = 0.8$ , the initial thickness  $h_0 = 8.29 \text{ cm}$ ,  $h_f/h_0 = 0.83$ , load = 10 kg.

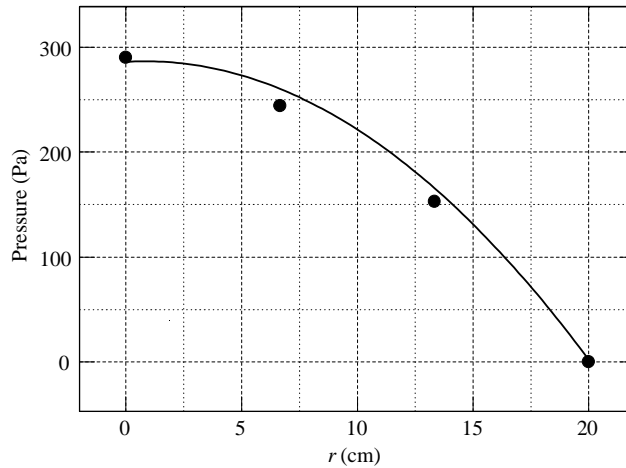


FIGURE 12. Theoretical prediction for the radial pressure distribution beneath the piston surface and its comparison with the experimental data at  $t = 1.40 \text{ s}$ , when the peak value of pressure is achieved. The initial Darcy permeability of snow is  $K_0 = 1.7 \times 10^{-8} \text{ m}^2$ , the initial porosity  $\phi_0 = 0.8$ , the initial thickness  $h_0 = 8.29 \text{ cm}$ ,  $h_f/h_0 = 0.83$ , load = 10 kg. ●,  $p-r$  relationship, experiment; —,  $p-r$  relationship, theory.

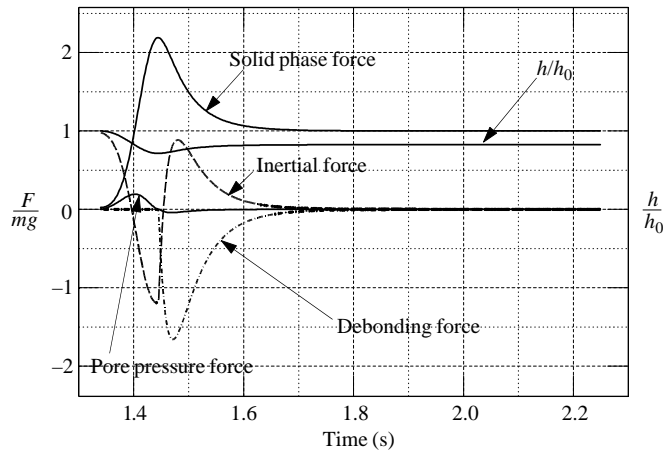


FIGURE 13. Time-dependent forces during dynamic compression of fresh snow.

figure 6, it is obvious that fresh snow is too porous to trap air efficiently and the damping effect from the pore air pressure is insufficient to dissipate the piston inertia on the rebound. The damping force from the debonding of the sintered crystals is required to balance the piston inertia. The fast relaxation time for the pore air pressure (0.1s) is also attributed to the high permeability and porosity of the fresh snow.

## 5. Concluding remarks

In this paper, we have developed a novel experimental and theoretical approach for examining the dynamic lift forces that are generated during rapid initial compaction under gravitational loading of both fresh powder snow and wind-packed older snow in a layer whose thickness is typical of a snow blanket that is left after a single snowfall in an urban environment. Our dynamic experiments provide the first measurements of the excess pore pressure that builds up inside a snow layer after a sudden compression by a falling planar surface and its subsequent decay owing to the venting of the air from the snow at the edges of the cylinder. The spatial distribution of the pore pressure was also measured. In static experiments, we have been able to separate out the force exerted by the solid phase (snow) as a function of its instantaneous deformation. The theoretical consolidation model provides excellent agreement with the experimental results if the initial Darcy permeability  $K_0$  is chosen in the correct range and the debonding effects of the sintered snow crystals are considered in the piston rebound. To our knowledge, this is the first time that such forces have been considered for other than a single ice crystal.

As described previously, there are at least four oversimplifications encountered in applying the present experiments to describe skiing: (i) the air resistance of the surrounding snow at the lateral edges of the skis is neglected; (ii) most skiing conditions involve a fresh snow layer on a packed base, which consists of recrystallized snow having a permeability that is 20–30 times smaller than fresh powder snow (Jordan 1999); (iii) the shear forces at the lateral edges of the skis have been neglected, though studies examining the deformation of the snow at the edge of a compression surface suggest this force is small (Shoop & Alger 1998); (iv) the inertia of the snow that is thrust out at the sides of the skis during manoeuvring turns has

not been considered. However, the present paper does qualitatively and quantitatively explore the time variation of the various dynamic forces that are encountered when a weighted planar surface is suddenly dropped on a snow layer before it is supported by the pressure bulb that develops in the ice crystal phase once quasi-steady longer-time settling is achieved. It confirms the basic physics in Feng & Weinbaum (2000) that on the time scale of importance for skiing or snowboarding on fine-grained wind-packed snow, the pressure of the transiently trapped air provides a significant fraction of the total lift even for small compressions. For skiing or snowboarding on fresh snow, the solid phase will carry a substantially greater portion of the load since the excess pore pressure will be insufficient to carry most of the load.

While the lubrication theory developed in FW illustrates the striking similarity between a red cell gliding over the endothelial surface layer (ESL) that lines human capillaries, and a person skiing, it does not provide a rigorous basis for evaluating its accuracy or limitations for the red cell, since its dimensions are obviously too small to obtain the detailed pressure measurements that would be needed for proper assessment. When the motion of a red cell is arrested, the time scale for the drainage of the fluid from the endothelial surface layer was determined by the observation that the gap between the red cell and endothelial cell membranes nearly vanishes in  $\sim 0.5$  s (Weinbaum *et al.* 2003). This characteristic time is very close to the pressure relaxation time that we found in the present dynamic compression study with wind-packed snow. The experimental and theoretical approach presented in this paper, thus, provides an intriguing analogue for the drainage of the ESL following red blood cell arrest.

One limitation in the present study is that the Darcy permeability of the snow was not measured in parallel experiments with the same snow sample to verify the theoretically predicted value of  $K_0$ . However, recently we carried out some measurements to determine the effects of compression on permeability of snow samples by using the apparatus described in Albert *et al.* (2000). Although the results of these experiments are not directly applicable to the present study, they clearly demonstrated that  $K_0$  is reduced by an amount that varies from 17 % to 50 % for a 20 % compression of various snow samples.

Another point of interest is the damping effect from the solid phase of fresh powder snow following maximum compression. This damping effect has been attributed to the breaking of ice crystal bonds during piston rebound and has been modelled by a force that is proportional to the instantaneous velocity of the piston by introducing a debonding coefficient  $\eta$ . This damping force can also be determined by applying an accelerometer to the piston. As observed in (2), there are three contributing forces, the inertial force of the piston, the pore air pressure and the ice crystal force, whose summation is equal to  $mg$  at any time during the compression process. The pore air pressure has already been measured in the dynamic experiment; the ice crystal force without the bond breakage effect was also measured in the static experiment. The accelerometer gives the measurement of the piston acceleration, which provides the magnitude of the inertial force. If the summation of these three measured forces is not equal to  $mg$  during the rebound, the imbalance can be attributed to the debonding force of the sintered ice crystals.

The phenomena of pore pressure increase due to sudden compression of soft porous media and that of slow pressure venting due to viscous effects which are described in the present work is a new concept. The application to snow compaction and the potential application to human skiing were chosen for their novelty. In a further study, we have applied this idea in the design of a future-generation train that can glide on a soft porous track whose mechanical properties are similar to goose down

(Wu *et al.* 2004). The key insight in the latter application is that one could greatly enhance the lift and reduce the drag due to friction in the solid phase if the lateral loss of pore pressure at the sidewalls of the track could be eliminated.

This research was performed in partial fulfilment of the requirements for the PhD degree from the City University of New York by Q. Wu who was supported in part by NIH grant 19544. The data acquisition software that was used in the dynamic compression experiments was developed by Minwei Gong, a PhD student at CCNY.

## REFERENCES

- ABELE, G. & GOW, A. 1975 Compressibility characteristics of undisturbed snow. *USA Cold Regions Res. Engng Lab. Res. Rep.* **336**.
- ABELE, G. & GOW, A. 1976 Compressibility characteristics of compacted snow. *USA Cold Regions Res. Engng Lab. Res. Rep.* **76-21**.
- ALBERT, D. G. 1993 A comparison between wave propagation in water-saturated and air-saturated porous materials. *J. Appl. Phys.* **73**, 28–36.
- ALBERT, M. R., GRANNAS, A. M., BOTTENHEIM, J., SHEPSON, P. B. & PERRON, F. E. 2002 Processes and properties of snow–air transfer in the high Arctic with application to interstitial ozone at Alert, Canada. *Atmos. Environ.* **36**, 2779–2787.
- ALBERT, M. R. & SHULTZ, E. F. 2002 Snow and firn properties and air–snow transport processes at Summit, Greenland. *Atmos. Environ.* **36**, 2789–2797.
- ALBERT, M. R., SHULTZ, E. F. & PERRON, F. E. 2000 Snow and firn permeability at Siple Dome, Antarctica. *Ann. Glaciol.* **31**, 353–356.
- ARONS, E. M. & COLBECK, S. C. 1995 Geometry of heat and mass transfer in dry snow: a review of theory and experiment. *Rev. Geophys.* **33**, 463–492.
- AUER, A. H. & VEAL, D. L. 1970 The dimensions of ice crystals in natural clouds. *Atmos. Sci.* **27**, 919–926.
- BEAR, J. 1972 *Dynamics of Fluids in Porous Media*. Elsevier.
- BIOT, M. A. 1941 General theory of three-dimensional consolidation. *J. Appl. Phys.* **12**, 155–164.
- BIOT, M. A. & WILLIS, D. G. 1957 The elastic coefficients of the theory of consolidation. *J. Appl. Mech.* **24**, 594–601.
- COLBECK, S. C. 1997 A review of sintering in seasonal snow. *USA Cold Regions Res. Engng Lab. Res. Rep.* **97-10**.
- FASSNACHT, S. R., INNES, J., KOUWEN, N. & SOULIS, E. D. 1999 The specific surface area of fresh dendritic snow crystals. *56th Eastern snow conference Fredericton, New Brunswick, Canada*.
- FENG, J. & WEINBAUM, S. 2000 Lubrication theory in highly compressible porous media: the mechanics of skiing, from red cells to humans. *J. Fluid Mech.* **422**, 282–317.
- GUBLER, H. 1982 Strength of bonds between ice grains after short contact times. *J. Glaciol.* **28**, 457–473.
- JOHNSON, J. B. 1982 On the application of Biot's theory to acoustic wave propagation in snow. *Cold Regions Sci. Technol.* **6**, 49–60.
- JOHNSON, J. B. 1991 Simple model of shock-wave attenuation in snow. *J. Glaciol.* **37**, 303–312.
- JORDAN, R. E., HARDY, J. P., PERRON JR, F. E. & FISK, D. J. 1999 Air permeability and capillary rise as measures of the pore structure of snow: an experimental and theoretical study. *Hydrol. Process.* **13**, 1733–1753.
- MELLOR, M. 1964 Properties of snow. *USA Cold Regions Res. Engng Lab. Monograph III-A1*.
- MELLOR, M. 1977 Engineering properties of snow. *J. Glaciol.* **19**, 15–66.
- ONO, A. 1970 Growth mode of ice crystals in natural clouds. *J. Atmos. Sci.* **27**, 649–658.
- SHAPIRO, L. H., JOHNSON, J. B., STURM, M. & BLAISDELL, G. L. 1997 Snow mechanics. Review of the state of knowledge and applications. *USA Cold Regions Res. Engng Lab. Res. Rep.* **97-3**.
- SHIMIZU, H. 1970 Air permeability of deposited snow. *Inst. Low Temp. Sci.: Sapporo, Japan, Contribution* **1053**, English Trans.

- SHOOP, S. & ALGER, R. 1998 Snow deformation beneath a vertically loaded plate formation of pressure bulb with limited lateral displacement. *9th Intl conf. on Cold Regions Engng, Duluth, MN*, 27–30 Sept. 1998.
- TERZAGHI, K. 1943 *Theoretical Soil Mechanics*. Wiley.
- WAKAHAMA, G. & SATO, A. 1977 Propagation of a plastic wave in snow. *J. Glaciol.* **19**, 175–183.
- WEINBAUM, S., ZHANG, X., HAN, Y., VINK, H. & COWIN, S. C. 2003 Mechanotransduction and flow across the endothelial glycocalyx. *Proc. Natl Acad. Sci.* **100**, 7988–7995.
- WU, Q., ANDREOPOULOS, Y. & WEINBAUM, S. 2004 From red cells to snowboarding: a new concept for a train track. *Phys. Rev. Lett.* **93**, 194501.
- YONG, R. N. & FUKUE, M. 1977 Performance of snow under confined compression. *J. Terramech.* **14**, 59–82.